Capacitive Transduction for Liquid Crystal Based Sensors, Part II: Partially Disordered System

Alaeddin S. Abu-Abed, *Member, IEEE*, and Robert G. Lindquist

***Abstract*—This paper presents the capacitive transduction technique involved with liquid crystal (LC) based sensors in partially disordered systems. These sensors have the potential applications in chemical and biological systems. The theory for tracking the average molecular deformation (state of alignment) and degree of ordering of anisotropic and partially disordered LC film via capacitive sensing is investigated. This system is modeled using the Q-tensor approach in modeling uniaxial LC material. The proposed sensor design is an interdigitated electrodes structure. Transverse and fringing capacitances as function of the molecular deformation are calculated. It is verified that three capacitance measurements are required to track the average molecular orientation and the degree of disorder in the LC film. The sensitivity for the sensor at different alignments and ordering degree is also studied. Toward practical sensor, neuro-fuzzy system is modeled to simulate the capacitive transduction and to monitor the LC profile. Sensors are fabricated and tested. Both the experimental and calculated capacitances are presented and compared.**

***Index Terms*—Biosensors, capacitive sensing, chemical sensors, liquid crystal (LC), neuro-fuzzy.**

I. Introduction

THE ability to detect and identify toxic chemicals, explosives, and biological agents at very low levels in gases, in liquids, and on surfaces in real time is of critical national importance. As a result, numerous sensors technologies have been investigated over the past decade in an effort to develop low cost, portable, field-deployable, highly selective chemical and biological sensors. Several of the more promising techniques involve liquid crystal (LC) based sensors [1]–[9]. In these sensors, the presence of a chemical or biological agent causes a change in the alignment of the liquid crystal material. Surface driven orientational changes in LC films have proven to be highly effective in amplifying the presence of targeted analytes in chemical and biological sensors [10]–[18]. The collective behavior and high anisotropy of the LC molecules allow for the detection of extremely low levels of targeted agents. For example, an LC-based chemical sensor capable of detecting parts per billion vapor concentrations of targeted low molecular weight molecules was developed in [10]. In all these sensors, optical transduction (visual inspection) has been used to sense the distortion within the LC material. The innovation of this two parts paper is to involve capacitive transduction in LC sensors.

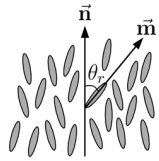

Fig. 1. Representation of the director axis, $\vec{n}$, and long molecule axis, $\vec{m}$.

Part I of this paper [19] introduces a capacitive transduction technique for ordered LC systems that offers advantages over the optical techniques. The capacitive technique offers the ability to identify and track the deformation rather than simply sensing an LC distortion. In addition, a simpler system with autonomous operation and reduced possible false alarms is achievable. In the previous work [19], the authors presented the theoretical and experimental principles of monitoring and tracking the nematic LC molecular profile via capacitive transduction in ordered systems. It was found that two capacitive measurements can uniquely track changes of the molecular orientation in an ordered LC film. Although the effort in [19] has been demonstrated in fully ordered systems, LC films in many practical sensors are partially disordered.

The key point of this paper is to extend the capacitive transduction method to handle uniformly and partially disordered anisotropic LC films. These techniques will lead to more practical and operative LC sensor systems [20]. The theory and experiments are expanded to handle partially disordered LC films. In this case, three capacitance measurements are required to track the average director axis and the order parameter.

A geometrical representation of a rod-like nematic molecular profile is illustrated in Section II. The theory to model the LC permittivity tensor is discussed in Section III, where the proposed sensor structure is introduced in Section IV. Capacitive modeling in the presence of partially disordered LC film is discussed in Section V. Monitoring LC molecular profile parameters via capacitive transduction utilizing ANFIS is discussed in Section VI. Section VII contains simulation and experimental results and discussion of these results while the summary of this work is presented in Section VIII.

II. Geometrical Representation of a Partially Disordered LC Molecular Profile

Ordered molecular orientation appears in LC film in which the molecules align parallel to a preferred direction. In real LC films, thermal energy causes the molecules to oscillate and the amount of orientational order degrades. In this case, the molecules have a random orientational behavior and are no longer aligned parallel to one another. At any point in the LC

Manuscript received January 30, 2008; revised March 11, 2008; accepted March 11, 2008. This work was supported by the National Science Foundation (NSF) under Award BES-0428073. The associate editor coordinating the review of this paper and approving it for publication was Prof. Evgeny Katz.

The authors are with the Electrical and Computer Engineering Department, The University of Alabama at Huntsville, Huntsville, AL 35899 USA (e-mail: abuabea1@eng.uah.edu; lindquis@ece.uah.edu).

Color versions of one or more of the figures in this paper are available online at http://ieeexplore.ieee.org.

Digital Object Identifier 10.1109/JSEN.2008.925451

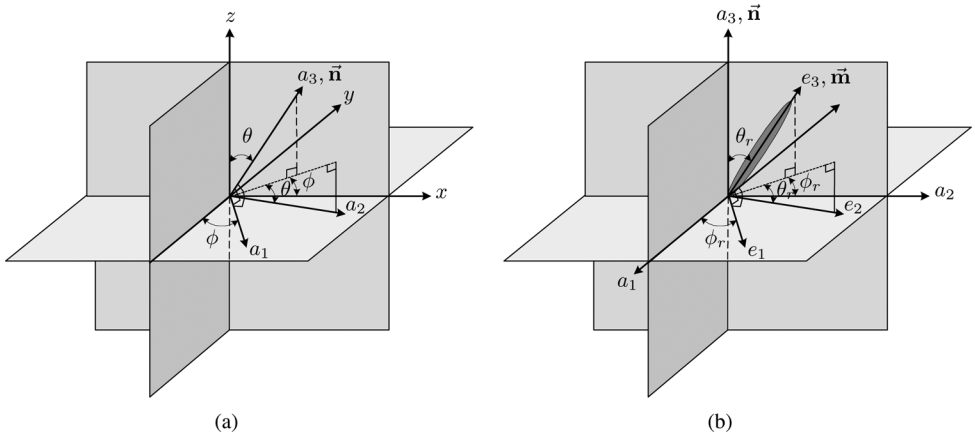

Fig. 2. Geometrical representation of the director axis and the rod-like molecule long axis.

film, a vector $\vec{\mathbf{n}}$ can be defined to represent the averaged molecular orientations around that point. An example of a partially disorder rod-like molecular orientation along the director axis is shown in Fig. 1, where $\vec{\mathbf{m}}$ and $\vec{\mathbf{n}}$ represent the individual long molecule axis and the director axis, respectively, and θ_r is the angle between them.

Realization of the geometrical representation of the director axis and the long molecule axis in a partially disordered LC material is helpful in interpreting the molecular deformation. This also facilitates treating the permittivity tensor as well as the order parameter inside the LC film. The director and the long molecule axes are the geometrical system used in tracking the director axis orientation and the order parameter via capacitive transduction.

A. Geometrical Representation of the Director Axis

The rectangular Cartesian coordinates x, y, and z are the lab frame references and a_1, a_2, and a_3 are the director principal axes such that the director axis is along a_3, as shown in Fig. 2(a). The director axis makes a zenithal angle, θ, with the z axis and an azimuthal angle, ϕ, between the projection of the director axis on the x-y plane and the x axis. The orientation matrix, $\mathbf{T}$, translates the field components from the Cartesian coordinate system to the director principal axes. Relying on Fig. 2(a), $\mathbf{T}$ can be expressed as

$$\mathbf{T} = \begin{bmatrix} \sin\phi & -\cos\phi & 0 \\ \cos\theta\cos\phi & \cos\theta\sin\phi & -\sin\theta \\ \sin\theta\cos\phi & \sin\theta\sin\phi & \cos\theta \end{bmatrix}. \tag{1}$$

B. Geometrical Representation of the Long Molecule Axis

A geometrical representation of the molecular principal axes with respect to the director principal axes is shown in Fig. 2(b). In this case, molecular principal axes are represented by e_1, e_2, and e_3, such that the long molecule axis is along e_3. The long axis of the rod-like molecule makes an angle θ_r with the director axis and an angle ϕ_r between projection of the long axis of the molecule on the a_1-a_2 plane and the a_2 axis.

Considering the stochastic behavior of the molecules in partially disordered LC film, θ_r and ϕ_r are treated as random variables with a joint probability density function $w(\theta_r, \phi_r)$ [21]. In fact, θ_r and ϕ_r are independent random variables, therefore, $w(\theta_r, \phi_r)$ can be written as $w(\theta_r, \phi_r) = f(\theta_r) \cdot g(\phi_r)$, where $f(\theta_r)$ and $g(\phi_r)$ are the marginal probability density functions of θ_r and ϕ_r, respectively. The orientation matrix, $\mathbf{R}$, that translates the field components from the director principal axes system to the molecular principal axes system can be expressed as

$$\mathbf{R} = \begin{bmatrix} \cos\phi_r & \sin\phi_r & 0 \\ -\cos\theta_r\sin\phi_r & \cos\theta_r\cos\phi_r & -\sin\theta_r \\ -\sin\theta_r\sin\phi_r & \sin\theta_r\cos\phi_r & \cos\theta_r \end{bmatrix}. \tag{2}$$

In the case of fully ordered LC film, all the molecules align parallel to each other and to the director axis. In this case, the same coordinate system can be used to represent both the director and the molecular principal coordinates. In the nematic LC phase, the rod-like molecules have complete cylindrical symmetry about the director axis, therefore, ϕ_r has uniform distribution in the domain $[0, 2\pi]$ and $g(\phi_r) = 1/2\pi$. Moreover, the orientational distribution function $w(\theta_r, \phi_r)$ depends only on the distribution function $f(\theta_r)$.

C. Molecular Profile Degree of Order

Although the director axis defines the average orientation of molecules in the nematic phase, it provides no information regarding the degree of orientational ordering. A scalar quantity is demanded to identify the spread of the molecules about the director axis and give information about the degree of order along the director axis. The scalar quantity is the order parameter and is used to quantify the long-range orientational order and define the degree of alignment in LCs. The order parameter, S, which defines the degree of alignment of the molecules, also depends on $f(\theta_r)$. The order parameter is defined according to the second order Legendre equation as

$$S = \frac{1}{2}\left\langle 3\cos^2\theta_r - 1 \right\rangle \tag{3}$$

where $\langle\cdot\rangle$ denotes a statistical average.

For perfectly parallel aligned LC film, θ_r goes to zero and the order parameter goes to one. In contrast, the order parameter turns towards zero in a completely random film. In this case, LC film is in the isotropic phase. In the nematic phase, order parameter has an intermediate value which is temperature dependent. A typical values for S at low temperatures are in the range between 0.3 and 0.7.

III. Developing the Permittivity Tensor Locally

Nematic LCs are anisotropic materials and most can be represented as a uniaxial crystal that exhibits two electrical permittivities, the parallel permittivity, $\epsilon_{||}$, for the electric field traveling in parallel with the molecule's long axis and the perpendicular permittivity, $\epsilon_{\perp}$, for the electric field traveling perpendicular to the molecule's long axis. In the molecular principal coordinate system, the permittivity tensor, ϵ_m, is given by

$$\epsilon_m = \epsilon_o \begin{bmatrix} \epsilon_{\perp} & 0 & 0 \\ 0 & \epsilon_{\perp} & 0 \\ 0 & 0 & \epsilon_{||} \end{bmatrix} \tag{4}$$

where ϵ_o is the dielectric constant in the free space.

Since the molecular profile is monitored with respect to the Cartesian coordinate system, the permittivity tensor is going to be calculated according to these axes. This necessitates the orientation matrix $\mathbf{H}$, such that $\mathbf{H} = \mathbf{R} \times \mathbf{T}$, to map the components of the field vectors from the lab frame to the molecular direction. The permittivity tensor, ϵ, in the Cartesian coordinates is

$$\epsilon = \epsilon_o \begin{bmatrix} \epsilon_{xx} & \epsilon_{xy} & \epsilon_{xz} \\ \epsilon_{yx} & \epsilon_{yy} & \epsilon_{yz} \\ \epsilon_{zx} & \epsilon_{zy} & \epsilon_{zz} \end{bmatrix} \tag{5}$$

where ϵ_{lk} is the individual permittivity such that $l, k = x, y$, or z. Recalling (4), ϵ can be rewritten as

$$\epsilon = \mathbf{H}^{-1} \epsilon_m \mathbf{H}. \tag{6}$$

$\mathbf{T}$ and $\mathbf{R}$ are orthogonal matrices, this makes $\mathbf{H}$ also orthogonal. Therefore, the inverse of the transformation matrix $\mathbf{H}$ is equal to the transpose of $\mathbf{H}$, i.e., $\mathbf{H}^{-1} = \mathbf{H}'$. Since the entries of $\mathbf{H}$ depend on θ_r and ϕ_r, these entries will be also handled as random variables. The individual dielectric constants in (5) will also be handled as random variables. Using the definition of the order parameter as in (3), the statistical average of the permittivity tensor given in (5) can be written as

$$\langle \epsilon \rangle = \bar{\epsilon} = \epsilon_o \begin{bmatrix} \bar{\epsilon}_{xx} & \bar{\epsilon}_{xy} & \bar{\epsilon}_{xz} \\ \bar{\epsilon}_{yx} & \bar{\epsilon}_{yy} & \bar{\epsilon}_{yz} \\ \bar{\epsilon}_{zx} & \bar{\epsilon}_{zy} & \bar{\epsilon}_{zz} \end{bmatrix} \tag{7}$$

where

$$\begin{aligned} \bar{\epsilon}_{xx} &= \frac{2\epsilon_{\perp} + \epsilon_{||}}{3} + S\Delta\epsilon \left(\sin^2\theta \cos^2\phi - \frac{1}{3} \right) \\ \bar{\epsilon}_{yy} &= \frac{2\epsilon_{\perp} + \epsilon_{||}}{3} + S\Delta\epsilon \left(\sin^2\theta \sin^2\phi - \frac{1}{3} \right) \\ \bar{\epsilon}_{zz} &= \frac{2\epsilon_{\perp} + \epsilon_{||}}{3} + S\Delta\epsilon \left(\cos^2\theta - \frac{1}{3} \right) \\ \bar{\epsilon}_{xy} &= \bar{\epsilon}_{yx} = S\Delta\epsilon \sin^2\theta \sin\phi \cos\phi \\ \bar{\epsilon}_{xz} &= \bar{\epsilon}_{zx} = S\Delta\epsilon \sin\theta \cos\theta \cos\phi \\ \bar{\epsilon}_{yz} &= \bar{\epsilon}_{zy} = S\Delta\epsilon \sin\theta \cos\theta \sin\phi \end{aligned} \tag{8}$$

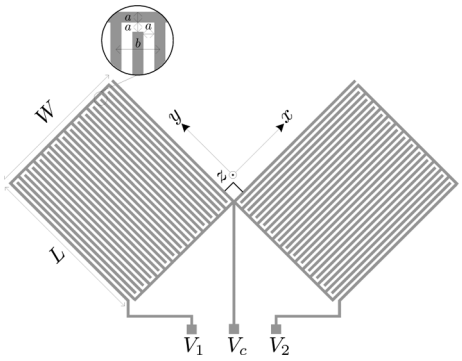

Fig. 3. Top view of the LC interdigitated sensor.

where $\bar{\epsilon}_{lk} = \langle \epsilon_{lk} \rangle$ is the statistical average of ϵ_{lk}. The average permittivity tensor, $\bar{\epsilon}$, can be simplified as

$$\bar{\epsilon} = \frac{2\epsilon_{\perp} + \epsilon_{||}}{3} \mathbf{I} + \Delta\epsilon \mathbf{Q} \tag{9}$$

where $\mathbf{I}$ is the identity tensor, $\Delta\epsilon = \epsilon_{||} - \epsilon_{\perp}$ is the dielectric anisotropy, and $\mathbf{Q}$ is called the Q-tensor [22] which is given by (10), shown at the bottom of the page. Notice that the Q-tensor has the following properties.

1) $\mathbf{Q}$ is function of S, θ and ϕ.
2) $\mathbf{Q}$ is traceless matrix.
3) Eigenvalues of $\mathbf{Q}$ are $(-S/3, -S/3, 2S/3)$.

IV. Sensor Structure

The interdigitated electrodes configuration can be used for tracking the average director axis of an LC film via capacitive sensing. A top view of a possible electrode design consists of two perpendicular interdigital cells is shown in Fig. 3. These interdigitated electrodes are patterned in one substrate where a continuous electrode is on the other substrate. An LC film of thickness d is sandwiched between these substrates as shown in Fig. 4. Fig. 3 shows a top view of two perpendicular interdigitated cells in x-y plane where these cells share a continuous electrode on the top. Fig. 4 shows cross section of one unit cell of the sensor in the x-z plane. The electric field lines which penetrate the LC film in this structure are either transverse or fringing lines similar to those illustrated in Fig. 4. The associated capacitances can be handled as two independent sets as shown in Fig. 5. The transverse capacitance between the interdigitated electrodes and the top electrode is denoted by C_{Ts} while the fringing capacitances between the different interdigitated electrodes are denoted by C_{F1s} and C_{F2s}.

The sensing mechanism in this case is similar to the mechanism discussed in [19] in the sense that it depends on transverse and fringing capacitance measurements. The transverse capacitance depends on the zenithal angle, θ, and the order parameter S, while the fringing capacitances are functions of the θ, ϕ, and S. By measuring these capacitances, the director orientation, θ

$$\mathbf{Q} = S \begin{bmatrix} \sin^2\theta\cos^2\phi - \frac{1}{3} & \sin^2\theta\sin\phi\cos\phi & \sin\theta\cos\theta\cos\phi \\ \sin^2\theta\sin\phi\cos\phi & \sin^2\theta\sin^2\phi - \frac{1}{3} & \sin\theta\cos\theta\sin\phi \\ \sin\theta\cos\theta\cos\phi & \sin\theta\cos\theta\sin\phi & \cos^2\theta - \frac{1}{3} \end{bmatrix} \tag{10}$$

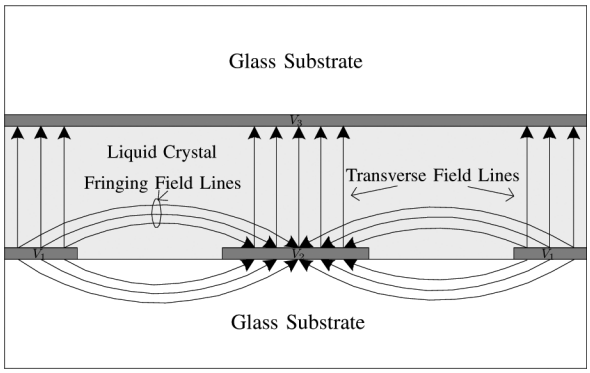

Fig. 4. Cross section of one unit cell of the sensor architecture.

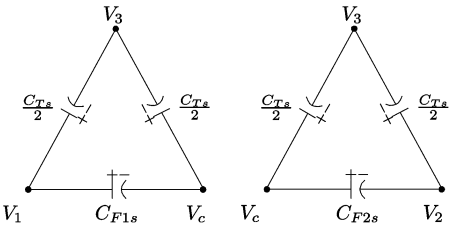

Fig. 5. Symbolic representation of the transverse and fringing capacitance between the sensor's electrodes.

and ϕ, as well as the order parameter can be determined. Thus, this structure could be used to track the director orientation and the degree of order by performing three independent capacitance measurements, $C_{Ts}(\theta, S)$, $C_{F1s}(\theta, \phi, S)$, and $C_{F2s}(\theta, \phi, S)$.

V. Capacitance Modeling

Although some techniques are used to derive closed form for the interdigitated structure capacitance associated with homogenous and isotropic material, such as conformal mapping [23], no closed form exists to calculate this capacitance in the presence of anisotropic material. In this section, a finite difference method (FDM) will be used to model the capacitances of the interdigital structure in the prepense of anisotropic LC material. The electric field in the LC film satisfies the Maxwell's equation

$$\nabla \cdot (\bar{\epsilon}\vec{E}) = 0 \tag{11}$$

where $\bar{\epsilon}$ is the average permittivity tensor given in (7) and $\vec{E}$ is the electric field vector. The permittivity tensor, $\bar{\epsilon}$, depends on the director axis orientation, θ and ϕ, and the molecular degree of order, S. The solution of Maxwell's equation will be evaluated in two different regions, inside the partially disordered LC film and in the isotropic glass substrate.

A. Solving (11) Inside the LC Film

Solving Maxwell's equation inside the LC film in Cartesian coordinate system requires the evaluation of the parameters given in (8). Recalling that $\vec{E} = -\nabla V$ and substituting (7) in (11), solving this equation in two dimensions (x and z, where $\partial/\partial y = 0$), Maxwell's equation in (11) ends up being

$$\bar{\epsilon}_{xx}\frac{\partial^2 V(x,z)}{\partial x^2} + 2\bar{\epsilon}_{xz}\frac{\partial^2 V(x,z)}{\partial x \partial z} + \bar{\epsilon}_{zz}\frac{\partial^2 V(x,z)}{\partial z^2} = 0 \tag{12}$$

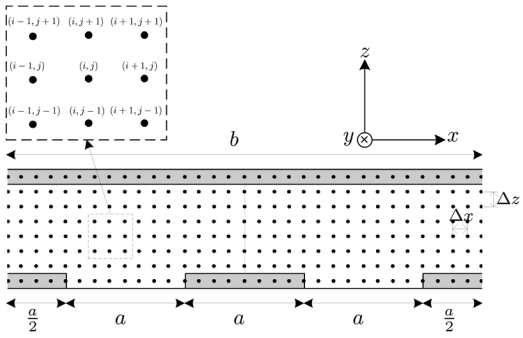

Fig. 6. Graphical display of one unit cell in a potential field that is divided into Δx and Δz regions to solve Maxwell's equation for $V_{i,j}$.

where $\bar{\epsilon}_{xx}$, $\bar{\epsilon}_{xz}$, and $\bar{\epsilon}_{zz}$ are the average individual permittivities given in (8). The partial differential equation in (12) is going to be solved by applying the FDM to evaluate $V(x, z)$. The FDM algorithm will evaluate the potential at specific points inside the LC film, where these potential values will be used later to calculate the capacitance between the electrodes. We first will consider the grid mesh in of the cross section given in Fig. 4 as shown in Fig. 6

Solving (12) for the potential at the (i, j) node, $V_{i,j}$, as a function of the permittivity tensor entries will give

$$\begin{aligned} V_{i,j} = {} & \bar{A}_x\left(V_{i+1,j} + V_{i-1,j}\right) + \bar{A}_z\left(V_{i,j+1} + V_{i,j-1}\right) \\ & + \bar{A}_{xz}\left(V_{i+1,j+1} - V_{i+1,j-1} - V_{i-1,j+1} + V_{i-1,j-1}\right) \end{aligned} \tag{13}$$

where

$$\begin{aligned} \bar{A}_x &= \frac{0.5\bar{\epsilon}_{xx}(\Delta z)^2}{\bar{\epsilon}_{xx}(\Delta z)^2 + \bar{\epsilon}_{zz}(\Delta x)^2} \\ \bar{A}_z &= \frac{0.5\bar{\epsilon}_{zz}(\Delta x)^2}{\bar{\epsilon}_{xx}(\Delta z)^2 + \bar{\epsilon}_{zz}(\Delta x)^2} \\ \bar{A}_{xz} &= \frac{0.25\bar{\epsilon}_{xz}\Delta x \Delta z}{\bar{\epsilon}_{xx}(\Delta z)^2 + \bar{\epsilon}_{zz}(\Delta x)^2}. \end{aligned} \tag{14}$$

B. Solving (11) Inside the Glass Substrate

As in [19], the solution in terms of the potential inside the glass substrate is given by

$$V_{i,j} = \frac{0.5(\Delta x)^2(\Delta z)^2}{(\Delta x)^2 + (\Delta z)^2}\left[\frac{V_{i+1,j} + V_{i-1,j}}{(\Delta x)^2} + \frac{V_{i,j+1} + V_{i,j-1}}{(\Delta z)^2}\right]. \tag{15}$$

Equations (13) and (15) will be used to calculate the electric field in a closed path around one of the electrodes in order to evaluate the capacitance as in [19]. The analysis is applied to one unit cell and by making full use of symmetry, the capacitance for the whole structure can be evaluated.

VI. Monitoring LC Molecular Profile Parameters Via Capacitive Measurements

The simulation calculates the capacitances of the sensor structure as functions of the LC profile parameters, i.e., θ, ϕ, and S. On the other hand, the practical use of the sensor is to measure the capacitance and provide information about the profile parameter. One of the practical ways to achieve this is

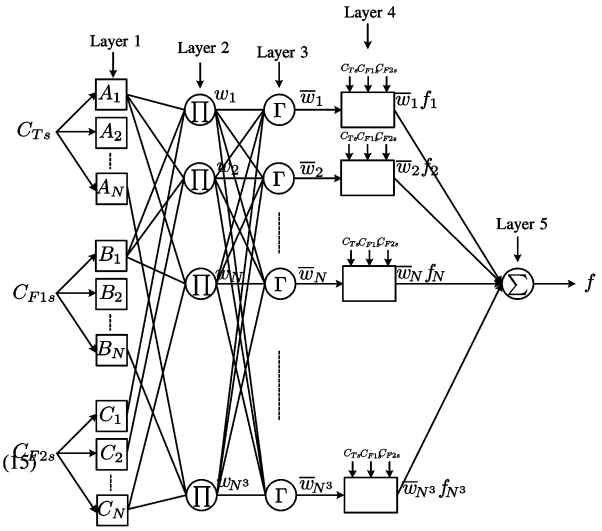

Fig. 7. Scheme of ANFIS architecture.

to build a model which can be provided by the capacitance to calculate the profile parameters. Our method is to design an artificial neuro-fuzzy network that can be trained off-line by utilizing the simulation part results to track and interpolate θ, ϕ, and S. The system under investigation in this paper is called adaptive neuro-fuzzy inference system (ANFIS).

A. ANFIS Architecture Design

ANFIS was created by R. Jang as a hybrid neuro-fuzzy system that utilizes Tsukamoto or Sugeno fuzzy models with appropriate membership functions embedded into artificial neural network [24]. Unlike the classical fuzzy systems introduced by L. Zadeh [25], ANFIS system is an adaptive network that requires training and hybrid learning before moving to the application phase. In this paper, we develop a first order Sugeno-type ANFIS model to monitor the LC profile. This model involves five layers that map multi inputs to a single output. The proposed three-input ANFIS architecture is schematized in Fig. 7.

This architecture has three inputs, C_{Ts}, C_{F1s}, and C_{F2s}, where each input is associated with N membership functions. Each ANFIS network ends up by N^3 rules, five layers, and one output, f. Since ANFIS is a single output network, three independent ANFIS models are developed where each model will track one parameter of the LC profile. The ANFIS model is built such that the output is a first order function of the inputs. The Sugeno-style if-then rules for this network have the general rule structure

$$\begin{aligned}&\text{IF } C_{Ts} \text{ is } A_m \text{ and } C_{Fs1} \text{ is } B_n \text{ and } C_{Fs2} \text{ is } C_k,\\ &\text{THEN } f_i = \alpha_i C_{Ts} + \beta_i C_{Fs1} + \gamma_i C_{Fs2} + \xi_i\end{aligned}$$

where $m, n, k = 1, 2, 3, \ldots, N$, where f_i is the output of the ith rule where $i = 1, 2, 3, \ldots, N^3$, and $\{\alpha_i, \beta_i, \gamma_i, \xi_i\}$ is the consequent parameters set of the ith rule. $\{A_1, A_2, \ldots, A_N\}$, $\{B_1, B_2, \ldots, B_N\}$, and $\{C_1, C_2, \ldots, C_N\}$ are the fuzzy sets associated with C_{Ts}, C_{Fs1}, and C_{Fs2}, respectively. The output of the first layer is the membership grade, i.e., μ_{A_m}, μ_{B_n}, or μ_{C_k}, in which the inputs, C_{Ts}, C_{Fs1}, and C_{Fs2}, belong to the fuzzy sets A_m, B_n, or C_k, respectively. The membership functions may be chosen from the appropriate list; for example, a generalized bell membership function associated with the fuzzy set A_m can be expressed by

$$\mu_{A_m}(C_{Ts}) = \frac{1}{1 + \left|\frac{C_{Ts} - c_m}{a_m}\right|^{2b_m}} \tag{16}$$

where a_m, b_m, and c_m are the parameters of the generalized bell membership function. The second's layer output is called the firing strength which is calculated by multiplying the incoming signals. The firing strength of the ith rule, w_i, is given by

$$w_i = \mu_{A_m}(C_{Ts}) \mu_{B_n}(C_{F1s}) \mu_{C_k}(C_{F1s}). \tag{17}$$

The third layer calculates the ratio of the ith rule firing strength to the sum of the firing strengths. The output of layer three shown in Fig. 7 is

$$\overline{w}_i = \frac{w_i}{\sum_{n=1}^{N^3} w_n}. \tag{18}$$

Layer four is called the adaptive layer. By using the consequent parameters set of the ith rule, $\{\alpha_i, \beta_i, \gamma_i, \xi_i\}$, the fourth output of this rule is

$$\overline{w}_i f_i = \overline{w}_i (\alpha_i C_{Ts} + \beta_i C_{F1s} + \gamma_i C_{F2s} + \xi_i). \tag{19}$$

The last layer output is calculated by adding all the incoming signals together, i.e., $f = \sum w_i f_i / \sum w_i$. This output can be rewritten as

$$f = \sum_{i=1}^{N^3} \overline{w}_i (\alpha_i C_{Ts} + \beta_i C_{F1s} + \gamma_i C_{F2s} + \xi_i) \tag{20}$$

where f could be θ, ϕ or S. By providing the input/output data set to the ANFIS algorithm, it should be able to calculate the optimum consequent parameters as well as the optimum membership function parameters.

B. ANFIS Training Phase: Building the System

As discussed earlier, a simulation code utilizing FDM is developed to calculate the capacitance of the interdigitated sensor structure in the presence of a partially disorder LC film. The simulation code is provided by θ, ϕ, and S to model the capacitances C_{F1s}, C_{F2s}, and C_{Ts}. ANFIS is trained to simulate the capacitive transduction technique to track the LC profile parameters by utilizing the measured capacitances.

In the training phase, each ANFIS system will be trained offline individually to track one parameter. This can be accomplished since θ, ϕ, and S are independent parameters. As illustrated in Fig. 8, each ANFIS model will be provided by the capacitances as the input set, and one of the profile parameters, i.e., θ, ϕ, or S as the output. The training will be continued and ANFIS output will be compared with the actual parameter and

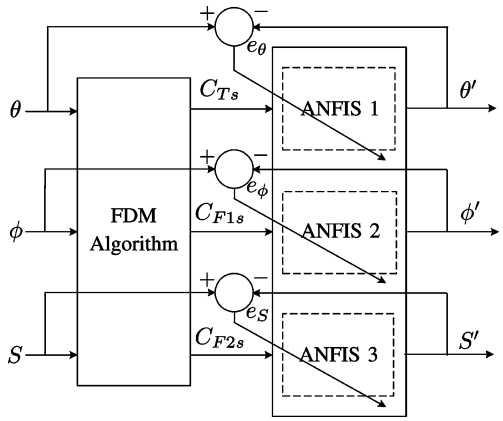

Fig. 8. Training phase of the ANFIS system designed to track θ, ϕ, and S.

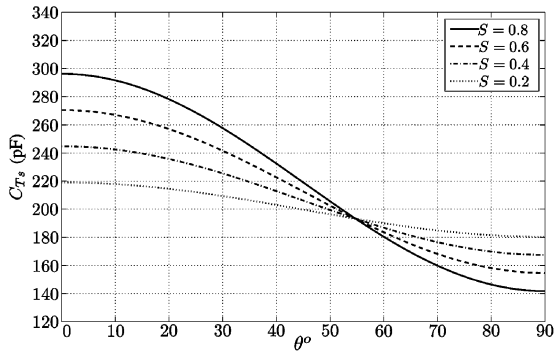

Fig. 9. Transverse capacitance, C_{Ts}, in pF as a function of θ at different order parameter values, for 5CB LC film.

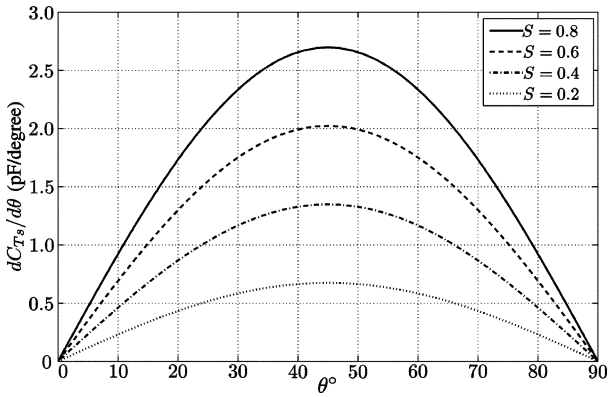

Fig. 10. Sensitivity, in pF/degree, of the transverse capacitance C_{Ts}, for 5CB LC film.

the error is calculated after each epoch. Training will be terminated when it satisfies the desired error. Once the desired error is met, ANFIS can be placed for use in the application phase.

C. ANFIS Application Phase: Tracking LC Profile Parameters

In this phase, three capacitance measurements will be experimentally performed and provided to ANFIS systems. Outputs will be the estimated values of the profile parameters, θ', ϕ', and S'. Numerical examples on using ANFIS in tracking the profile parameters will be discussed in Section VII.

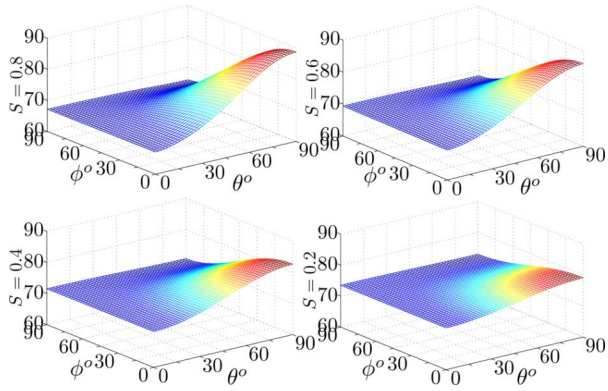

Fig. 11. Fringing capacitance, C_{F1s}, in pF as a function of θ and ϕ at different order parameter values, for 5CB LC film.

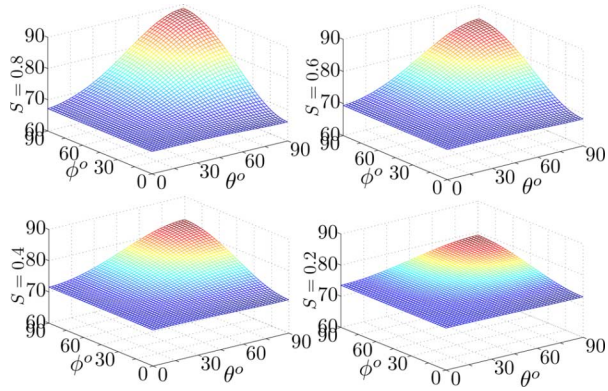

Fig. 12. Fringing capacitance, C_{F2s}, in pF as a function of θ and ϕ at different order parameter values, for 5CB LC film.

VII. Simulation and Experimental Results

In this section, simulation and experimental results are presented to provide insight into capacitive transduction for the electrode design shown in Fig. 3. The 5CB LC is used to simulate and calculate the capacitances. The results show that the transverse capacitance C_{Ts} depends only on the zenithal angle, θ, and the order parameter, S. The transverse capacitance as a function of θ at different order parameter values is shown in Fig. 9. A prior knowledge of how the orientation of the LC molecules will likely reorient in response to some environmental stimulus is critical to optimizing the performance of the sensor. The electrode structure and the initial state of orientation impact the sensitivity. The sensitivity of the transverse field capacitance for different values of S as a function of θ is shown in Fig. 10. It is shown that sensitivity decreases as the system becomes more disordered, i.e., S decreases.

Both of the fringing capacitances depend on θ, ϕ, and S. The modeled fringing capacitances C_{F1} and C_{F2} as functions of θ and ϕ at $S = 0.2$, 0.4, 0.6, and 0.8 are shown in Figs. 11 and 12, respectively. The sensitivity of the fringing field capacitance is a function of both the zenithal and azimuthal angles. Figs. 13 and 14 illustrate the sensitivity of the fringing field capacitance, at different S values, as a function of the azimuthal angle given

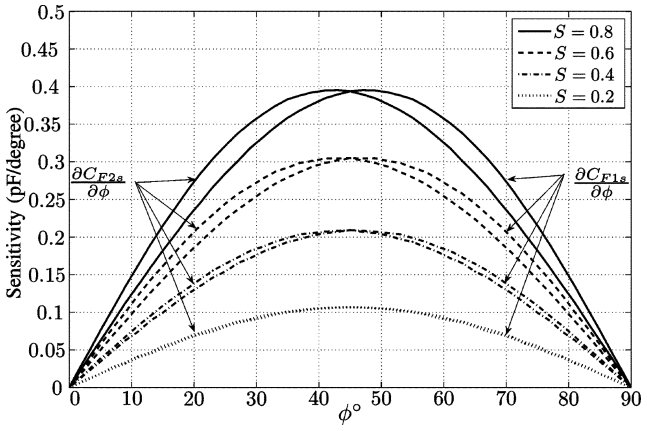

Fig. 13. Sensitivity, in pF/degree, of C_{F1s} and C_{F2s} at $\theta = 90°$ at different values of the order parameter, for 5CB LC film.

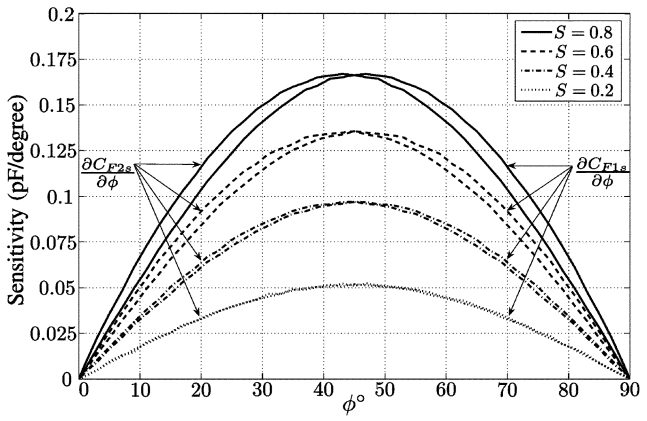

Fig. 14. Sensitivity, in pF/degree, of C_{F1s} and C_{F2s} at $\theta = 45°$ at different values of the order parameter, for 5CB LC film.

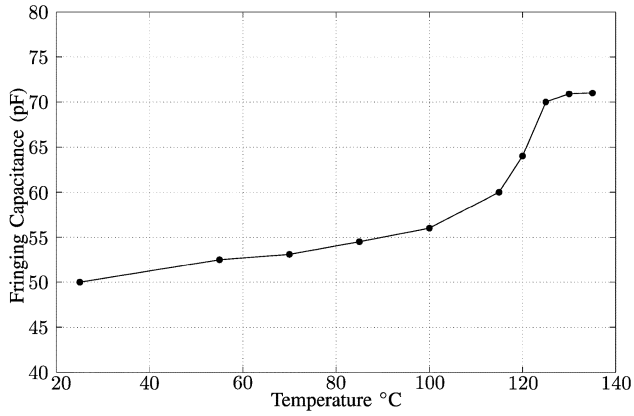

Fig. 15. Measured capacitance, in pF, at different temperature values of BL006 LC film when the initial director is at $\theta = \phi = 90°$.

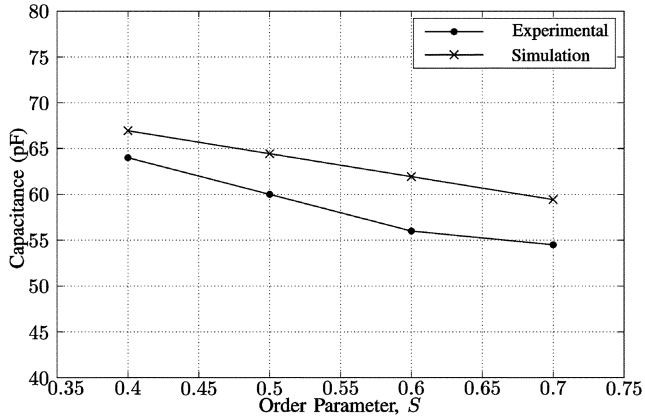

Fig. 16. Experimental and calculated capacitance, in pF, at different order parameter values of BL006 LC film when the initial director is at $\theta = \phi = 90°$.

the zenithal angle is 90° and 45°, respectively. As expected, at a given S and ϕ, the sensitivity is at a maximum when $\theta = 90°$.

The behavior of the sensor in the presence of nematic LC film was investigated experimentally. 5 mm $\times$ 5.5 mm interdigitated structures with 10 μm width fingers and 10 μm spacing between fingers have been fabricated and tested. A thick ($\sim 51\ \mu$m) film of BL006 (MERCK) liquid crystal has been used to cover the upper surface of these sensors. The molecules were aligned to behave in a homeotropic and different homogenous orientations. Experimental results for these profiles were discussed in [19]. In this paper, the capacitance is measured by exposing the LC film to heat, this will reduce the order of the molecules and as a result the capacitance will change accordingly.

The capacitance was measured at different values of temperature. It is known that increasing the BL006 LC temperature will decrease the order parameter. This will increase the capacitance when the initial condition is at $\theta = \phi = 90°$ as shown in Fig. 15. When the temperature reaches the clearing point, the molecules will behave isotropically. Since the order parameter depends on the temperature, the order parameter at different temperature values is extracted [26], and the capacitance as function of the order parameter is plotted in Fig. 16. Three ANFIS architectures are developed and trained to monitor 5CB LC film profile in partially disorder state. Six generalized bell membership functions

TABLE I
ACTUAL AND ESTIMATED LC FILM ORIENTATION PARAMETERS USING ANFIS

Actual Parameters			Measured Capacitances			Estimated Parameters		
θ	ϕ	S	C_{Ts} (pF)	C_{F1s} (pF)	C_{F2s} (pF)	θ'	ϕ'	S'
90^o	90^o	1.00	128.83	63.79	91.19	89.00^o	89.27^o	1.000
37.16^o	16.82^o	0.95	248.63	72.57	66.15	38.30^o	14.94^o	0.952
65.43^o	23.16^o	0.85	166.88	81.76	68.98	65.17^o	24.13^o	0.844
19.45^o	57.12^o	0.75	273.78	68.45	69.29	19.55^o	62.73^o	0.745
90^o	57.12^o	0.65	151.36	93.66	81.36	88.72^o	57.82^o	0.648
90^o	0^o	0.55	157.80	85.09	68.97	87.61^o	2.63^o	0.552
31.76^o	10.18^o	0.45	227.11	74.14	70.97	31.1^o	7.71^o	0.446
33.16^o	87.12^o	0.35	218.08	71.88	74.78	35.24^o	87.18^o	0.346
82.73^o	45^o	0.25	177.9	76.22	76.21	84.13^o	44.95^o	0.229
78.52^o	73.15^o	0.15	184.72	73.96	77.64	78.46^o	75.19^o	0.157

are assigned to each input to give a precise estimation for θ, ϕ, and S. Some examples of the actual and tracked (estimated) values of the order parameter and the director axis orientation in a partially disordered 5CB LC film are given in Table I.

VIII. SUMMARY

The method of capacitive transduction for LC-based sensors has been presented and tested. Test cells are shown in Fig. 17. Sensors with interdigitated electrodes can be used to monitor the profile of a partially disordered nematic LC film. Three capacitance measurements are required to track the LC molecular average orientation and the order parameter. Adaptive neuro-fuzzy inference systems (ANFIS) are designed, trained, and tested to

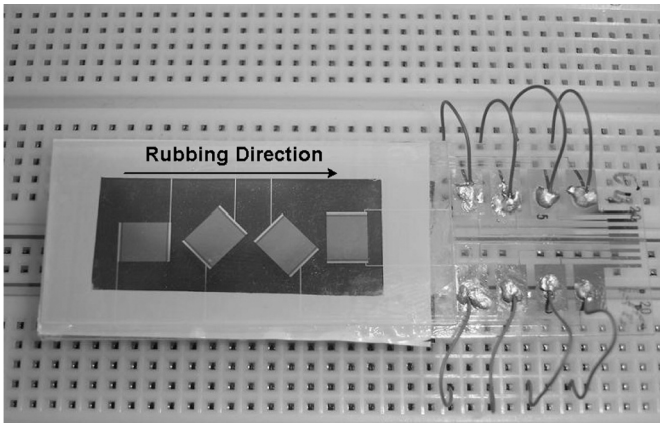

Fig. 17. Test cells of the LC based sensor.

monitor the LC profile parameters utilizing capacitance measurements. ANFIS proves the capability to monitor the LC profile via capacitive transduction technique.

REFERENCES

[1] D. Villalta, P. B. Romelli, C. Savina, N. Bizzaro, R. Tozzoli, E. Tonutti, A. Ghirardello, and A. Doria, "Anti-dsDNA antibody avidity determination by a simple reliable ELISA method for SLE diagnosis and monitoring," *Lupus*, vol. 12, no. 1, pp. 31–36, 2003.

[2] J. Chung, S. Park, D. Kim, J. Rhim, I. Kim, I. Choi, K. Yi, S. Ryu, P. Suh, D. Chung, Y. Bae, Y. Shin, and S. Park, "Identification of antigenic peptide recognized by the anti-JL1 leukemia-specific monoclonal antibody from combinatorial peptide phage display libraries," *J. Cancer Res. Clin. Oncol.*, vol. 128, no. 12, pp. 641–649, 2002.

[3] S. Poole, Y. Mistry, C. Ball, D. Gaines, E. Rose, L. P. Opie, G. Tucker, and M. Patel, "A rapid 'one-plate' in vitro test for pyrogens," *J. Immunol. Meth.*, vol. 274, no. 1–2, pp. 209–220, 2003.

[4] M. C. Kibbey, D. MacAllan, and J. W. Karaszkiewicz, "Novel electrochemiluminescent assays for drug discovery," *J. Assoc. Lab. Automat.*, vol. 5, no. 1, pp. 45–48, 2000.

[5] T. M. Kijek, C. A. Rossi, D. Moss, R. W. Parker, and E. A. Henchal, "Rapid and sensitive immunomagnetic-electrochemiluminescent detection of staphylococcal enterotoxin B," *J. Immunol. Meth.*, vol. 236, no. 1–2, pp. 9–17, 2000.

[6] R. M. Carter, R. C. Blake, T. D. Nguyen, and L. A. Bostanian, "Near real-time biosensor-based detection of 2,4-dinitrophenol," *Biosens. Bioelectron.*, vol. 18, no. 1, pp. 69–72, 2003.

[7] A. Ahmad, A. Ramakrishnan, M. A. McLean, and A. P. Breau, "Use of surface plasmon resonance biosensor technology as a possible alternative to detect differences in binding of enantiomeric drug compounds to immobilized albumins," *Biosens. Bioelectron.*, vol. 18, no. 4, pp. 399–404, 2003.

[8] L. Rasooly and A. Rasooly, "Real time biosensor analysis of staphylococcal enterotoxin a in food," *Int. J. Food Microbiol.*, vol. 49, no. 3, pp. 119–127, 1999.

[9] E. Howe and G. Harding, "A comparison of protocols for the optimisation of detection of bacteria using a surface acoustic wave (SAW) biosensor," *Biosens. Bioelectron.*, vol. 15, no. 11–12, pp. 641–649, 2000.

[10] R. Shah and N. L. Abbott, "Principles for measurment of chemical exposure based on recognition-driven anchoring transitions in liquid crystals," *Science*, vol. 293, no. 5533, pp. 1296–1299, 2001.

[11] J. Brake, M. Daschner, and N. L. Abbott, "Biomolecular interactions at phospholipid decorated surfaces of thermotropic liquid crystals," *Science*, vol. 302, no. 5653, pp. 2094–2097, 2003.

[12] R. R. Shah and N. L. Abbott, "Coupling of the orientations of liquid crystals and electrical double layers formed by the dissociation of surface-immobilized salts," *J. Phys. Chem. B*, vol. 105, no. 21, pp. 4936–4950, 2001.

[13] R. R. Shah and N. L. Abbott, "Using liquid crystals to image reactants and products of acid-base reactions on surfaces with micrometer resolution," *J. Amer. Chem. Soc.*, vol. 121, no. 49, pp. 11300–11310, 1999.

[14] Z. Hou, N. L. Abbott, and P. Stroeve, "Self-assembled monolayers on electroless gold impart pH-Responsive transport of ions in porous membranes," *Langmuir*, vol. 16, no. 5, pp. 2401–2404, 2000.

[15] V. K. Gupta and N. L. Abbott, "Uniform anchoring of nematic liquid crystals on self-assembled monolayers formed from alkanethiols on obliquely deposited films of gold," *Amer. Phys. Soc. Phys. Rev. E*, vol. 54, no. 5, pp. 4540–4543, 1996.

[16] V. K. Gupta, T. B. Dubrovsky, and N. L. Abbott, "Optical amplification of ligand-receptor binding using liquid crystals," *Science*, vol. 279, no. 5359, pp. 2077–2080, 1998.

[17] J. A. Van Nelson, S. R. Kim, and N. L. Abbott, "Amplification of specific binding events between biological species using lyotropic liquid crystals," *Langmuir*, vol. 18, no. 13, pp. 5031–5035, 2002.

[18] J. J. Skaife and N. L. Abbott, "Quantitative interpretation of the optical textures of liquid crystals caused by binding of immunoglobulins to surface-bound antigens," *Langmuir*, vol. 16, no. 7, pp. 3529–3536, 2000.

[19] A. Abu-Abed, R. G. Lindquist, and W.-H. Choi, "Capacitive transduction for liquid crystal based sensors, part I: Ordered systems," *IEEE Sensors J.*, vol. 7, no. 12, pp. 1617–1624, Dec. 2007.

[20] A. Abu-Abed, R. G. Lindquist, S. Jovanov, E. Jovanov, J. Namkung, and N. Abbott, "Capacitive based liquid crystal chemical and biological sensors," in *Proc. 6th IEEE Conf. Sensors*, Atlanta, GA, Oct. 2007.

[21] P. G. de Gennes and J. Prost, *The Physics of Liquid Crystals*, 2nd ed. Oxford, U.K.: Oxford Science, 1993.

[22] E. G. Virga, *Variational Theories for Liquid Crystals*. London, U.K.: Chapman & Hall, 1994.

[23] G. Ghione and C. Naldi, "Coplanar waveguides for MMIC applications: Effect of upper shielding, conductor backing, finite-extent ground planes, and line-to-Line coupling," *IEEE Trans. Microw. Theory Tech.*, vol. MTT-35, no. 3, pp. 260–267, 1987.

[24] J. S. R. Jang, C. Sun, and E. Mizutani, *Neuro Fuzzy and Soft Computing*. Englewood Cliffs, NJ: Prentice-Hall, 1997.

[25] L. A. Zadeh, "Fuzzy sets," *Inf. Contr.*, vol. 8, pp. 338–353, 1965.

[26] W. H. de Jeu, *Physical Properties of Liquid Crystalline Materials*. New York: Gordon and Breach, 1980.

Alaeddin S. Abu-Abed (S'04–M'08) received the B.Sc. and M.Sc. degrees from the Jordan University of Science and Technology, Irbid, Jordan, in 1999 and 2001, respectively, and the Ph.D degree from the University of Alabama at Huntsville (UAH), in 2007, all in electrical engineering.

He is currently a Visiting Assistant Professor in the Electrical and Computer Engineering Department, UAH, and Research Scientist in the Nano and Micro Device Center (NMDC), UAH. His major research interests include micro and nano devices, liquid crystal components and sensors, biological and chemical sensors, nanophotonics, and wireless communication.

Robert G. Lindquist received the Ph.D. degree from The Pennsylvania State University, Philadelphia, in 1992.

He is presently the Director of the Center for Applied Optics and a Professor of Electrical and Computer Engineering, The University of Alabama, Huntsville (UAH). His major research interests include liquid crystal devices for optical networking, chemical and biological sensors using liquid crystals, electronics on glass, photonics, and micro and nanofabrication technologies. Prior to UAH, he worked for Corning, Inc., where he managed a liquid crystal development group and worked as a Senior Research Scientist.